JOURNAL OF GEOPHYSICAL RESEARCH, VOL. 105, NO. D24, PAGES 29,475–29,488, DECEMBER 27, 2000

Estimating scalar sources, sinks, and fluxes in a forest canopy using Lagrangian, Eulerian, and hybrid inverse models

Mario Siqueira,[1,2] Chun-Ta Lai,[1] and Gabriel Katul[1,2]

Abstract. A new method was developed to estimate canopy sources and sinks from measured mean concentration profiles within the canopy (referred to as the "inverse" problem). The proposed method combined many of the practical advantages of the Lagrangian localized near-field (LNF) theory and higher-order Eulerian (EUL) closure principles. Particularly, this "hybrid" method successfully combined the essential conservation equations of closure modeling and the robustness of the regression source inversion developed for LNF theory. The proposed method along with LNF and EUL were tested using measurements from two field experiments collected in a pine forest and published measurements from a wind tunnel experiment. The field experiments were conducted to investigate the vertical distribution of the scalar fluxes within the canopy and the temporal patterns of the scalar fluxes above the canopy. This comparison constitutes the first "inverse method" comparison performed using the same data sets on all three models. For the wind tunnel data, all three models well reproduced the measured flux distribution. For the field experiments, all three models recovered the measured spatial and temporal flux distribution in an ensemble sense. The agreement between these three models is desirable to the inverse problem because it adds the necessary confidence in the computed flux distributions. However, the agreement among all three models with the field measurements, on a 30-min time step, was less than satisfactory. Additionally, the divergence between models and measurements increased with departure from a near-neutral atmospheric state. Despite fundamental differences in these model approximations, this similarity in model performance suggests that the source information recovered from a measured one-dimensional mean concentration profile will not be further enhanced by a one-dimensional steady state, planar homogeneous model of neutral flows.

1. Introduction

Estimating carbon dioxide (CO_2) source and sink (S_c) distribution and vertical fluxes (F_c) within and above forested canopies continues to be a critical research problem in biosphere-atmosphere exchange processes [*Wofsy et al*., 1993; *Gao et al*., 1993; *Vermetten et al*., 1994; *Baldocchi and Harley*, 1995; *Culf et al*., 1997; *Baldocchi and Meyers*, 1998; *Simpson et al*., 1998; *Lee*, 1998; *Rannik*, 1998; *Malhi et al*., 1998; *Potosnak et al*., 1999; *Gu et al*., 1999; *Anthoni et al*., 1999; *Law et al*., 1999]. It is impractical to measure the distribution of S_c beyond the leaf scale. On the other hand, in field experiments, the mean CO_2 concentration ($\bar{c}$) profiles are often measured within the canopy. Since sources and fluxes are directly related by a scalar concentration budget equation, the problem is in inferring S_c from the readily measured $\bar{c}$. This problem is commonly termed the "inverse problem" [*Raupach*, 1988, 1989a, 1989b] and is the subject of the present investigation.

Early attempts to estimate S_c from $\bar{c}$ relied on the so-called "K theory", which relates F_c to the vertical gradient of $\bar{c}$ via eddy diffusivity ($K_m(z)$). With this approximation, $S_c = -\partial/\partial z\,[K_m(z)\,\partial\bar{c}/\partial z]$, where z is the height above the ground surface. However, for the turbulent transport within vegetation, a local imbalance between turbulent production and dissipation commonly exists, which can lead to "countergradient" fluxes and the ultimate failure of K theory. The limitations of K theory are now well recognized [e.g., *Raupach*, 1988] (see review by *Wilson* [1989]) and have been documented by many field experiments [e.g., *Denmead and Bradley*, 1985] and laboratory studies [e.g., *Coppin et al*., 1986].

Over the past two decades, two basic approaches emerged to circumvent the limitations of K theory: Lagrangian dispersion models (e.g., localized near-field theory (LNF)) and higher-order Eulerian closure models. The LNF approach proposed by *Raupach* [1989a, 1989b] has been successfully used to infer S_c and F_c from measured $\bar{c}$ in many field experiments [*Raupach et al*., 1992; *Denmead*, 1995; *Katul et al*., 1997a; *Massman and Weil*, 1999; R. Leuning et al., (Source/sink distributions of heat, water vapor, carbon dioxide and methane in a rice canopy estimated using Lagrangian dispersion analysis, submitted to *Agricultural Forest Meteorology*, 2000)].

As discussed by *Katul and Albertson* [1999], the LNF approach does not allow for nonzero vertical velocity skewness, strong inhomogeneity in vertical source strength, and mean horizontal velocity variation within the canopy. These limitations were practically addressed via a second-order Eulerian closure "inverse" model (hereinafter referred to as EUL) recently proposed by *Katul and Albertson* [1999]. However, their inverse model calculations of S_c and F_c are sensitive to mea-

[1]School of the Environment, Duke University, Durham, North Carolina.
[2]Department of Civil and Environmental Engineering, Duke University, Durham, North Carolina.

Paper number 2000JD900543.
0148-0227/00/2000JD900543$09.00

surement errors in $\bar{c}$ (at least when compared to LNF). This sensitivity is attributed to the lack of any redundancy in the inversion for S_c from measured $\bar{c}$ by the EUL method.

Given the advantages and disadvantages of EUL and LNF, the next logical step in inverse modeling is the development of a new method that retains the advantages of both. Here a hybrid Eulerian/Lagragian (HEL) method is proposed to complement the existing LNF and EUL. Developing a spectrum of inverse models with different approximations provides synergies not attainable with a single model; that is, agreement between source or flux profiles computed using several inverse methods sensitive to different approximations provides some confidence that the recovered source or flux profile is not too sensitive to a particular model approximation. Disagreements between these models can also flag some uncertainties about the recovered source or flux profile. Hence the objective of this study is to contrast the skill of HEL, LNF, and EUL using the same data sets. All three methods will be compared using the wind tunnel heat dispersion measurements of *Coppin et al*. [1986] and the extensive F_c and $\bar{c}$ measurements collected at the Duke Forest near Durham, North Carolina.

2. Experiment

2.1. Study Site

Two sets of experiments were conducted at the Blackwood Division of the Duke Forest near Durham, North Carolina (36°02′N, 79°8′W, elevation = 163 m). The first set is a heat dispersion experiment aimed at assessing how well the models recover the vertical flux distribution within the canopy. The second set is a long-term CO_2 dispersion experiment aimed at assessing how well the models recover the temporal patterns of the CO_2 flux above the canopy.

The stand is a uniformly planted loblolly pine (*Pinus* taeda *L*.) forest that extends 300–600 m in the east-west direction and 1000 m in the north-south direction. The mean canopy height was 14.0 m (±0.5 m) in 1998. Topographic variations within the stand are small (terrain slope changes <5%) such that the influence of topography on the turbulent fluxes can be neglected [*Kaimal and Finnigan*, 1994].

2.2. Heat Dispersion Experiment

To assess the vertical distribution of scalar fluxes inside the canopy, simultaneous mean temperature profiles and turbulence statistics were measured inside the canopy. The mean temperature was measured at eight levels (1.5, 3.5, 5.5, 7.5, 9.5, 11.5, 13.5, and 15.5 m) using shielded copper Constantan thermocouples (20 gage, diameter = 0.812 mm). For this field setup, the thermocouples were sampled every 1 s and averaged every 1800 s (30 min). The thermocouples were calibrated in a water bath, and the maximum differences between them did not exceed 0.1°C. The calibration spanned a temperature range from 5° to 40°C.

The velocity statistics and turbulent heat flux distribution were simultaneously measured at 3.0, 4.9, 8.6, 10.9, 12.2, and 15.5 m above the forest floor using six Campbell Scientific triaxial sonic anemometers (CSAT3) (Campbell Scientific, Logan, Utah). The sampling frequency was 10 Hz and the sampling period was 1800 s (30 min) per run. More than 80 such runs were collected between April 19 and 23, 2000, for a wide range of stability conditions. Thirty runs with near-neutral condition above the canopy were identified and an ensemble of velocity statistics and sensible heat flux profiles was defined. The stability regime was determined using the stability parameter $\zeta = -(z - d)/L$, where d is the zero-plane displacement (determined from the momentum flux profile), L is the Obukhov length determined from the friction velocity (u_*) and sensible heat flux (H) measured above the canopy. Neutral conditions were assumed to occur for $|\zeta| < 0.05$.

2.3. CO_2 Dispersion Experiment

To assess the applicability of these three methods in reproducing the temporal patterns of scalar fluxes above the canopy, a long-term record of CO_2 fluxes above the canopy and mean CO_2 concentration profiles within the canopy were used. This data set is being collected as part of an ongoing long-term CO_2 flux monitoring initiative at the Duke AmeriFlux site [*Katul et al*., 1999; *Lai et al*., 2000].

The CO_2 fluxes above the canopy were measured by an eddy-covariance system comprised of a Licor-6262 CO_2/H_2O infrared gas analyzer (LI-COR, Lincoln, Nebraska) and a Campbell Scientific triaxial sonic anemometer. Figure 1 shows the experimental setup and the instrument heights relative to the canopy. The CSAT3 was positioned at 15.5 m above the ground surface and was anchored on a horizontal bar extending 1.5 m away from the walk-up tower top. The infrared gas analyzer was housed in an enclosure 4.5 m from the inlet cup, which was positioned just under the CSAT3. The sampling flow rate for the gas analyzer is 1.5×10^{-4} m^3 s^{-1}, sufficient to maintain turbulent flow in the tubing. A krypton hygrometer (KH2O, Campbell Scientific) was colocated with the CSAT3 to estimate the magnitude of tube attenuation and lag time between vertical velocity and scalar concentration fluctuations as discussed by *Katul et al*. [1997a, 1997b].

The analog signals from these instruments were sampled at 10 Hz using a Campbell Scientific 21X data logger with all digitized signals transferred to a computer via an optically isolated RS232 interface for future processing. All the 10 Hz raw measurement processing was performed using the procedures described by *Katul et al*. [1997a, 1997b] with scalar covariance computed after maximizing the cross correlation between vertical velocity fluctuations and CO_2 concentration fluctuations for each 30 min run. Other measurement and processing corrections were described by *Katul et al*. [1997a, 1997b].

A multiport system was installed to measure the mean CO_2 concentration inside the canopy at seven levels above the ground surface (3.5, 5.5, 7.5, 9.5, 11.5, 13.5, and 15.5 m). The concentration at each level was sampled for 60 s (45 s sampling and 15 s purging) at the beginning, the middle, and the end of a 30 min sampling duration by another Licor 6262 housed in a wooden shed 15 m away from the tower. The flow rate within the tube (internal diameter = 4.23 mm) was set at 1.5×10^{-5} m^3 s^{-1} to dampen all turbulent fluctuations.

The shoot silhouette area index, a value analogous to the leaf area index (LAI), was measured in the vertical at increments of 1 m by a pair of Licor LAI 2000 plant canopy analyzers 4 times a year starting in 1996. A subset of this data set was used to generate the flow statistics needed by all three methods. In a first-order analysis, to model the flow field, it was assumed that the LAI 2000 plant canopy analyzer measurement is analogous to the leaf area density $a(z)$.

2.4. Wind Tunnel Experiment

The wind tunnel experiment comprised a planar heat source located at $z/h = 0.8$ within a set of strips spaced in a regular

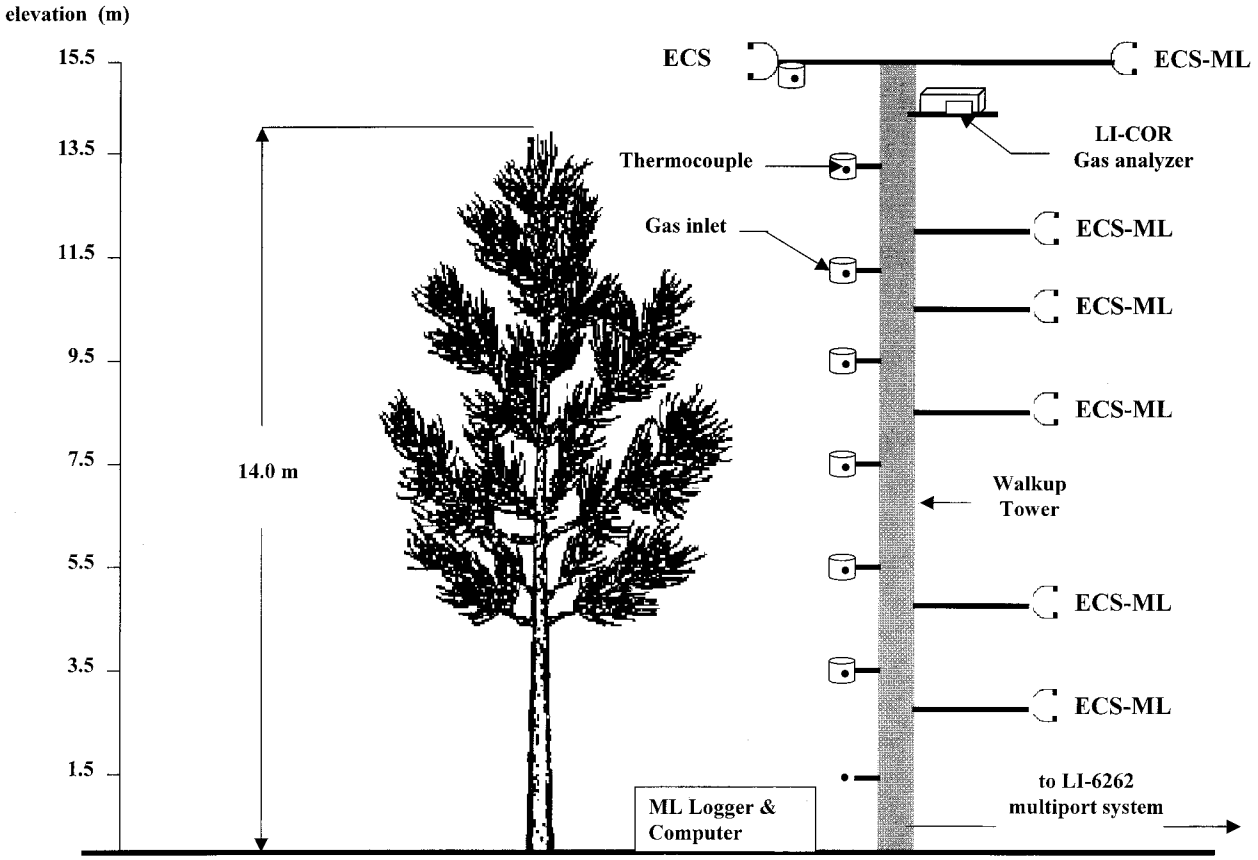

Figure 1. Experimental setup at the Duke Forest. The ECS stands for eddy-covariance system and ML for instruments used in the multilevel heat dispersion experiment.

diamond array with roughness concentration of 0.23 [*Coppin et al*., 1986]. The heat source was generated by an array of heated wires placed between the strips. In this experiment, temperature profiles in concert with sensible heat flux and velocity statistics were measured downwind. For this study, these temperature, sensible heat flux, and velocity statistics profiles were digitized from figures by *Raupach* [1989a] and *Coppin et al*. [1986]. These three experiments were used to evaluate the performance of the three inverse models described in section 3.

3. Theory

In this section the fundamentals of canopy scalar transport in the Eulerian and Lagrangian framework are reviewed to emphasize the key equations in EUL and LNF. The proposed hybrid method is then developed from these equations.

3.1. Scalar Transport in the Eulerian Frame of Reference

Applying time and horizontal averaging, the steady state scalar conservation equation for planar homogeneous high Reynolds and Peclet numbers flow (neglecting molecular diffusion) can be written as [*Finnigan*, 1985; *Raupach*, 1988]

$$\frac{\delta\langle\bar{c}\rangle}{\delta t} = 0 = -\frac{\delta\langle\overline{w'c'}\rangle}{\delta z} + S_c. \tag{1}$$

The overbar and angle brackets denote time and horizontal averaging respectively [*Raupach and Shaw*, 1982] and primes denote fluctuations from time averages; c is the scalar concentration (or temperature in the case of heat transport), w is the vertical velocity, and $F_c = \langle\overline{w'c'}\rangle$ is the vertical turbulent flux.

The corresponding time and horizontally averaged conservation equation for the vertical scalar flux budget is

$$\frac{\partial\langle\overline{w'c'}\rangle}{\partial t} = 0 = -\langle\overline{w'^2}\rangle\frac{\partial\langle\bar{c}\rangle}{\partial z} - \frac{\partial\langle\overline{w'w'c'}\rangle}{\partial z} - \left\langle\overline{c'\frac{\partial p'}{\partial z}}\right\rangle. \tag{2}$$

In (2), buoyancy, scalar drag, and waving source production were neglected. The three terms on the right-hand side of (2) represent the production of turbulent flux due to interactions between the turbulent flow and the mean concentration gradient, transport of the turbulent flux, and destruction by the pressure-scalar interaction, respectively.

The last two terms on the right-hand side of (2) are unknowns requiring closure approximations. In this study we adopt the transport term derived by *Meyers and Paw U* [1987] and the dissipation term modeled after *Finnigan* [1985]. These approximations are

$$\langle\overline{w'w'c'}\rangle = \frac{\tau}{C_8}\left[-\langle\overline{w'w'w'}\rangle\frac{\partial\langle\bar{c}\rangle}{\partial z} - \langle\overline{w'c'}\rangle\frac{\partial\langle\overline{w'w'}\rangle}{\partial z} - 2\langle\overline{w'w'}\rangle\frac{\partial\langle\overline{w'c'}\rangle}{\partial z}\right] \tag{3}$$

$$\left\langle\overline{c'\frac{\partial p'}{\partial z}}\right\rangle = C_4\frac{\langle\overline{w'c'}\rangle}{\tau}. \tag{4}$$

In (3) and (4), C_4 and C_8 are closure constants and τ is a Eulerian relaxation timescale given by

$$\tau = \frac{q^2}{\langle \varepsilon \rangle}, \tag{5}$$

where q $(= \sqrt{\langle \overline{u_i' u_i'} \rangle})$ is a characteristic turbulent velocity, $\langle \varepsilon \rangle$ is the mean rate of viscous dissipation, and u_i are the velocity components in the x_1 (or x), x_2 (or y), and x_3 (or z) directions, respectively, with x_1 aligned along the mean wind direction so that $\overline{u_2} = 0$.

Upon combining (2), (3), and (4), a second-order ordinary differential equation (ODE) can be derived for the scalar turbulent flux [*Katul and Albertson*, 1999]

$$A_1(z) \frac{d^2 \langle \overline{w'c'} \rangle}{dz^2} + A_2(z) \frac{d \langle \overline{w'c'} \rangle}{dz} + A_3(z) \langle \overline{w'c'} \rangle = A_4(z), \tag{6}$$

where

$$A_1(z) = \frac{2\tau}{C_8} \langle \overline{w'w'} \rangle,$$

$$A_2(z) = \frac{\tau}{C_8} \frac{d \langle \overline{w'w'} \rangle}{dz} + 2 \frac{d}{dz} \left(\frac{\tau}{C_8} \langle \overline{w'w'} \rangle \right),$$

$$A_3(z) = \frac{d}{dz} \left(\frac{\tau}{C_8} \frac{d \langle \overline{w'w'} \rangle}{dz} \right) - C_4 \frac{1}{\tau},$$

$$A_4(z) = \langle \overline{w'w'} \rangle \frac{d \langle \bar{c} \rangle}{dz} - \frac{d}{dz} \left(\frac{\tau}{C_8} \langle \overline{w'w'w'} \rangle \right) \frac{d \langle \bar{c} \rangle}{dz} - \left(\frac{\tau}{C_8} \langle \overline{w'w'w'} \rangle \right) \frac{d^2 \langle \bar{c} \rangle}{dz^2}.$$

The measured mean concentration profile is used only to calculate its gradient and curvature in $A_4(z)$, the nonhomogeneous term of the ODE in (6). The flow statistics $\langle \overline{w'w'} \rangle$, $\langle \overline{w'w'w'} \rangle$, and τ can be estimated using second-order closure principles such as the model proposed by *Wilson and Shaw* [1977] (reviewed in Appendix A). This closure model was tested at another location within the same pine forest and was shown to reproduce well the measured first and second moments of the velocity statistics [*Katul and Chang*, 1999]. Finally, (6) can be numerically solved for $\langle \overline{w'c'} \rangle$, which upon differentiation with respect to z results in the distribution of S_c. The boundary conditions for (6) are

$$z \geq h: \langle \overline{w'c'} \rangle = \frac{A_4(h)}{A_3(h)}, \qquad z = 0: \frac{d \langle \overline{w'c'} \rangle}{dz} = 0, \tag{7}$$

where h is the canopy height.

Equations (6) and (7) constitute the EUL inverse model of *Katul and Albertson* [1999]. The advantage of the EUL approach is its ability to incorporate non-Gaussian w statistics (e.g., nonzero $\overline{w'w'w'}$ in A_4) and advective scalar transport, two mechanisms that are neglected in the LNF approach of *Raupach* [1989a, 1989b], reviewed in section 3.2.

3.2. Lagrangian Localized Near-Field Theory

The localized near-field (LNF) theory calculates the mean scalar concentration relative to a reference value $\langle \bar{c} \rangle_R$ measured above the canopy at some reference height (z_R; $z_R > h$) by superimposing near-field (C_n) and far-field (C_f) contributions:

$$\langle \bar{c} \rangle - \langle \bar{c} \rangle_R = C_n + C_f. \tag{8}$$

As shown by *Raupach* [1989a, 1989b], the near-field contribution is computed via a kernel function:

$$C_n(z) = \int_0^\infty \frac{S_c(z_0)}{\sigma_w(z_0)} \left[k_n \left(\frac{z - z_0}{\sigma_w(z_0) T_L(z_0)} \right) + k_n \left(\frac{z + z_0}{\sigma_w(z_0) T_L(z_0)} \right) \right] dz_0, \tag{9}$$

where $\sigma_w (= \sqrt{\langle \overline{w'w'} \rangle})$ is the vertical velocity standard deviation and T_L is the Lagrangian integral timescale. An analytical approximation for the kernel function k_n was derived by *Raupach* [1989a] and is given by

$$k_n(\xi) = -0.39894 \ln (1 - e^{-|\xi|}) - 0.15623 e^{-|\xi|}. \tag{10}$$

This approximation was the subject of a recent study by *Gu* [1998] who concluded that the error in concentration could be as large as 6% if (10) is used. He suggested an alternative kernel function, which was considered unphysical by *Raupach* [1998].

The far-field contribution is calculated using the result from near field and a gradient-diffusion relationship such that

$$C_f(z) = \langle \bar{c} \rangle_R - C_n(z_R) + \int_z^{z_R} \frac{\langle \overline{w'c'} \rangle}{K_f(z)} dz. \tag{11}$$

In addition, neglecting the vertical velocity skewness, the far-field diffusivity K_f can be approximated by

$$K_f(z) = \sigma_w^2(z) T_L(z), \tag{12}$$

if the inhomogeneity is not too strong.

The Lagrangian integral timescale T_L, which is a measure of the persistence of the turbulent motion, is an intrinsically Lagrangian quantity and cannot be easily inferred from the commonly measured Eulerian velocity statistics. However, *Raupach* [1989a] suggested that T_L might be of the same order as the canopy timescale h/u_* (also discussed by *Raupach et al.* [1996]) such that

$$\frac{T_L(z) u_*}{h} = \beta, \tag{13}$$

where β is a constant.

The inverse calculation is performed by first dividing the canopy into m layers, each having an unknown uniform strength source. Next, the dispersion matrix is computed from

$$D_{ij} = \frac{\langle \bar{c} \rangle_i - \langle \bar{c} \rangle_R}{s \Delta z_j}, \tag{14}$$

where subscripts $i = 1, 2, \ldots; n$ and $j = 1, 2, \ldots; m$ represent the concentration and the source layers, respectively; D_{ij} are the elements of the dispersion matrix (m by n); s is an assumed source strength, and Δz_j are the source layer thickness. In (14) the $\langle \bar{c} \rangle_i$ are concentrations calculated from (8) assuming each source layer contributes individually to the concentration. Once the dispersion matrix is determined, the

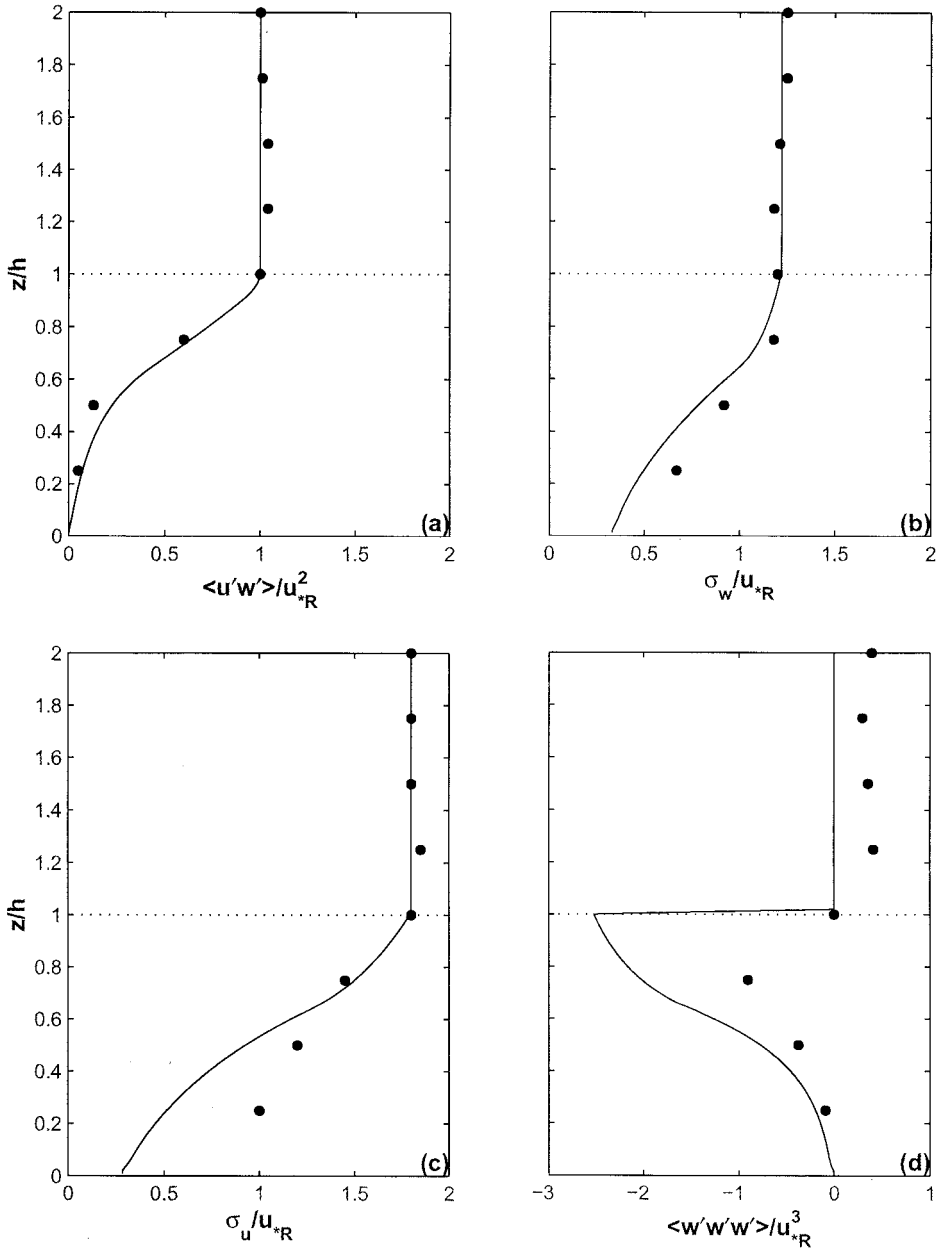

Figure 2. Comparison between measured (dots) and modeled (solid line) normalized velocity statistics using the *Wilson and Shaw* [1977] closure scheme for the wind tunnel experiment: (a) Reynolds stress, (b) vertical velocity standard deviation, (c) longitudinal velocity standard deviation, (d) third moment of vertical velocity. The normalizing variables are canopy height (h) for length and friction velocity (u_{*R} at $z/h = 1$) for velocity.

source strengths S_j can be computed from the measured mean concentration using

$$\langle \bar{c} \rangle_i - \langle \bar{c} \rangle_R = \sum_{j=1}^{m} D_{ij} S_j \Delta z_j, \tag{15}$$

where as before, m is the number of source layers and, in contrast to (14), $\langle \bar{c} \rangle_i$ are now the measured mean concentrations at the n levels. *Raupach* [1989a] found that the solution to (15) is sensitive to measurement errors when $m = n$.

To avoid such instability, redundant concentration measurements are necessary (i.e., $n > m$). As shown by *Raupach* [1989a], such redundancy reduces (15) to a regression problem with the source strengths calculated by a least squares approach:

$$\sum_{k=1}^{m} A_{jk} S_k = B_j \qquad (j = 1, \ldots, m), \tag{16}$$

where

$$A_{jk} = \sum_{i=1}^{n} D_{ij} \Delta z_j D_{ik} \Delta z_k,$$

$$B_j = \sum_{i=1}^{n} (C_i - C_R) D_{ij} \Delta z_j. \tag{17}$$

The above regression procedure provides some desirable "robustness" to the LNF method by decreasing its sensitivity to

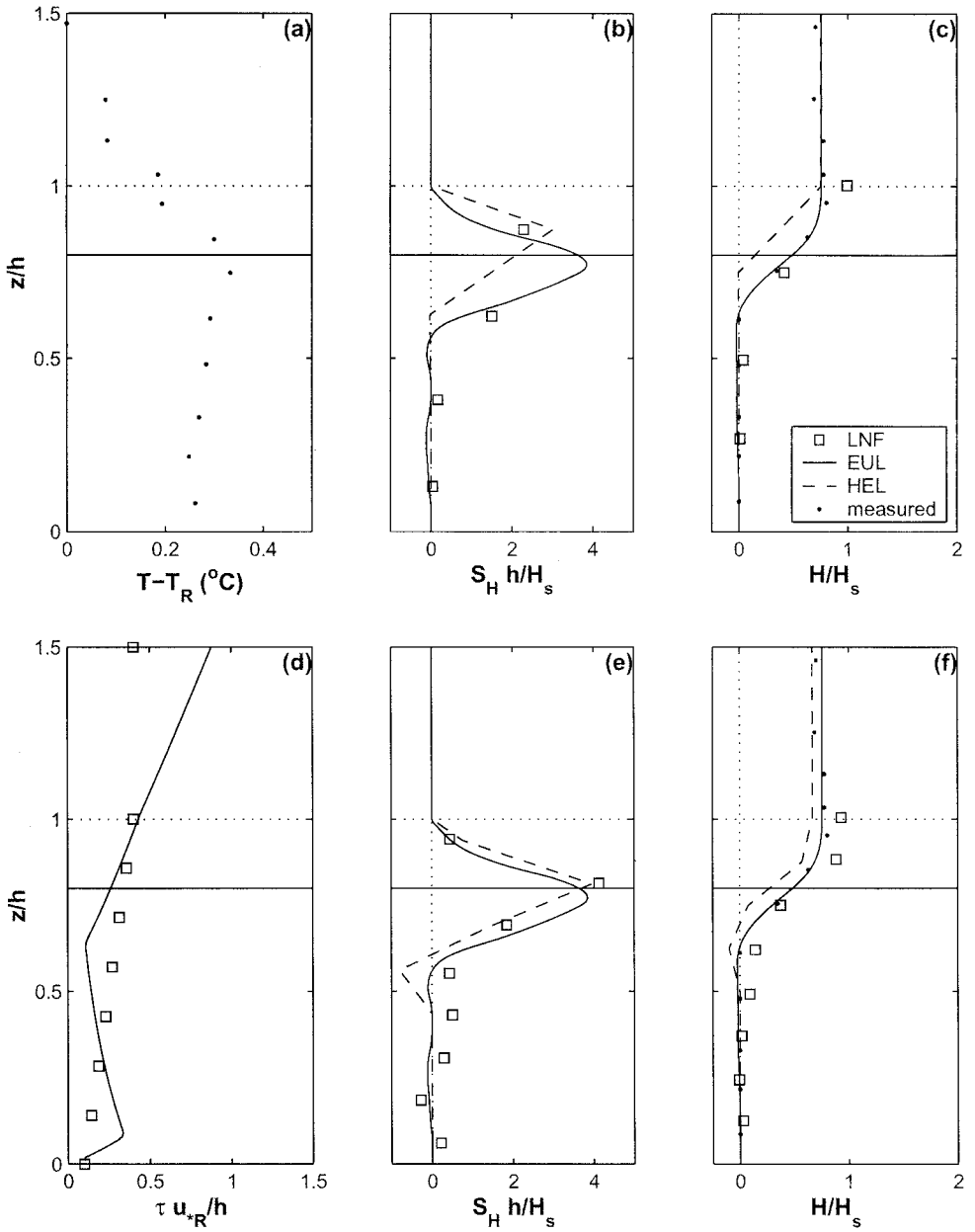

Figure 3. Comparison between measured and modeled sources and fluxes by EUL (solid line), LNF (squares), and HEL (dashed line) for the wind tunnel experiment. For LNF and HEL, the top panels are computations performed with four layers and the bottom panels are for computations performed using eight layers. The EUL is shown in both for reference. (a) Measured temperature profile from *Raupach* [1989a]. (b, e) Source comparisons by the three methods normalized by the source strength H_s and canopy height h. The source location is at $z/h = 0.8$ (horizontal solid line). (c, f) Normalized flux comparisons for the three methods with *Coppin et al.* [1986] sensible heat flux measurements (dots). (d) Relaxation timescale τ (line) and the Lagrangian integral timescale T_L (squares) both normalized by u_{*R}/h. Subscript R refers to the variable value at $z/h = 1$.

measurement errors. However, such an approach, when applied to a limited sample size (i.e., the number of measurements within the canopy is small), does not impose any smoothness constraints on the source. In other words the source variation can be unrealistically large between two adjacent levels [*Katul et al.*, 2000]. A smoothness constraint can be additionally imposed on (16) and (17) using the weighted measures of length procedure described in Appendix B [after *Menke*, 1989]. Hereinafter we refer to the LNF calculations constrained by this smoothness condition as LNF modified.

3.3. Hybrid Eulerian-Lagrangian Method

As evidenced from sections 3.1 and 3.2, both EUL and LNF possess strengths and limitations. While LNF is robust in the sense that it minimizes the effects of measurement errors on the estimation of S_c, it assumes a locally homogeneous near-field source and a Gaussian distributed w'. These approximations are clearly in contrast to many canopy turbulence experiments [*Raupach*, 1988]. Particularly, the skewness in w' is necessary to the sustainability of the ejection-sweep cycle re-

sponsible for much of the scalar transport in canopies [*Katul et al*., 1997b; *Blanken et al*., 1998]. The EUL approach circumvents such limitations, but the S_c computed from EUL is sensitive to errors in concentration measurements. Hence a hybrid scheme is proposed, in which the robustness of LNF, the smoothness imposed by the weighted measures of length algorithm, and the nonzero skewness in w' are retained, and the need for a local homogeneity assumption in the near-field source is alleviated.

The hybrid Eulerian-Lagrangian (HEL) approach adopts the second-order closure model described in section 3.1 to estimate the elements of the dispersion matrix in (15) and computes S_c from the regression algorithm of (17) modified by the smoothness condition. The second-order ODE, describing the concentration profile from a prescribed unit source (and hence the flux as in (1)), can be derived from (2), (3), and (4) and is given by

$$B_1(z)\frac{d^2\langle\bar{c}\rangle}{dz^2} + B_2(z)\frac{d\langle\bar{c}\rangle}{dz} = B_3(z), \tag{18}$$

where

$$B_1(z) = \frac{\tau}{C_8}\langle\overline{w'w'w'}\rangle,$$

$$B_2(z) = -\langle\overline{w'w'}\rangle + \frac{d}{dz}\left(\frac{\tau}{C_8}\langle\overline{w'w'w'}\rangle\right),$$

$$B_3(z) = -\frac{d}{dz}\left[\frac{\tau}{C_8}\left(\langle\overline{w'c'}\rangle\frac{d\langle\overline{w'w'}\rangle}{dz} + 2\langle\overline{w'w'}\rangle\frac{d\langle\overline{w'c'}\rangle}{dz}\right)\right] + C_4\frac{\langle\overline{w'c'}\rangle}{\tau}.$$

In (18), $\langle\overline{w'c'}\rangle$ is the turbulent flux profile calculated by integrating the unit source placed at one layer via (1); that is, the elements of D_{ij} are computed (1) by positioning a unit source at a layer located at node j, (2) integrating this source profile to obtain the $\langle\overline{w'c'}\rangle$ profile, and (3) solving the ODE in (18) for the concentration at all i nodes ($i = 1, \ldots, n$) resulting from the source placed at node j. This procedure is repeated for $j = 1, \ldots, m$ to obtain all the elements of the D_{ij} matrix needed in (16) and (17). The HEL scheme embeds the robustness of the LNF regression in the inversion but uses a forward calculation of D_{ij} that retains the effects of $\langle\overline{w'w'w'}\rangle$ through the coefficients B_1 and B_2. It is important to note that Lagrangian random flight models [e.g., *Thomson*, 1987] have been developed to account for non-Gaussian turbulent flows; however, these models require a large number of particles and are "stochastically" noisy [*Raupach*, 1988].

Table 1. Closure Constants and Other Empirical Parameters Used in the EUL, LNF, and HEL Parameterization for the Wind Tunnel (WT) and Duke Forest (DF) Experiments

Model	Constants for WT	Constants for DF
Momentum Closure Model	$(\sigma_u/u_*) = 1.80$	$(\sigma_u/u_*) = 2.20$
	$(\sigma_v/u_*) = 1.60$	$(\sigma_v/u_*) = 2.20$
	$(\sigma_w/u_*) = 1.22$	$(\sigma_w/u_*) = 1.10$
	$a_1 = 0.37$	$a_1 = 0.30$
	$a_2 = 0.79$	$a_2 = 2.00$
	$a_3 = 12.21$	$a_3 = 17.97$
	$C_w = 0.048$	$C_w = 0.061$
	$C_d = 1.0$	$C_d = 0.2$
	$\alpha = 0.008$	$\alpha = 0.02$
LNF	$(T_L u_*/h) = 0.1 + 0.4\, z/h$	$(T_L u_*/h) = 0.1$
Scalar Closure Models	$C_4 = 2.0$	$C_4 = 2.5$
	$C_8 = 9.0$	$C_8 = 9.0$

The parameters a_1, a_2, a_3, and C_w are computed from the normalized σ_u, σ_v, and σ_w as described by *Katul and Albertson* [1999]. The normalized σ_u, σ_v, and σ_w in the wind tunnel are different from the field experiments.

Table 2. Comparison Between Normalized Measured and Modeled Sensible Heat Flux Profiles for the *Coppin et al*. [1986] Experiment

Method	Slope A	Intercept B	rmse	R
LNF 8 layers	0.952	0.042	0.056	0.994
LNF 4 layers	0.869	0.045	0.088	0.983
EUL	1.028	−0.014	0.026	0.999
EUL ($\overline{w'w'w'} = 0$)	1.010	−0.024	0.035	0.998
HEL 8 layers	0.969	−0.044	0.105	0.977
HEL 4 layers	0.802	−0.036	0.189	0.926

The regression model is of the form $y = Ax + B$, where y is the modeled and x is the measured heat flux. The root-mean-square error (rmse) and the correlation coefficient R are also shown.

4. Results and Discussion

In this section, comparison among the predicted sources, sinks, and fluxes by LNF, EUL, and HEL for the *Coppin et al*. [1986] wind tunnel experiment, and the Duke Forest experiments are discussed.

4.1. Wind-Tunnel Heat Dispersion Experiment

Since EUL and HEL require a relaxation timescale (τ), vertical velocity standard deviation (σ_w) (also needed by LNF) and vertical velocity third moment ($\langle\overline{w'w'w'}\rangle$), we matched *Wilson and Shaw*'s [1977] model to the reported velocity statistics of *Coppin et al*. [1986] and *Raupach* [1988]. The comparisons between modeled and measured Reynolds stress ($\langle\overline{u'w'}\rangle$), longitudinal velocity standard deviation (σ_u), σ_w, and $\langle\overline{w'w'w'}\rangle$ are shown in Figure 2. For the second moments, the agreement between calculated and measured velocity statistics is sufficiently adequate for modeling the scalar transport. However, the model overestimated the magnitude of measured $\langle\overline{w'w'w'}\rangle$. Because of this overestimation, the sensitivity of the computed fluxes to variations in $\langle\overline{w'w'w'}\rangle$ is later investigated.

Using the measured temperature profile of *Raupach* [1989a] and the modeled velocity statistics in Figure 2, the heat sources and fluxes are computed using all three methods and com-

Table 3. Comparison Between Measured and Modeled Sensible Heat Flux Profiles for the Heat Dispersion Field Experiment

Method	Slope	Intercept	rmse	R
LNF modified	1.26	−13.68	55.86	0.85
LNF	1.59	−17.24	86.95	0.83
EUL	0.93	−11.81	40.21	0.87
HEL	1.00	−15.33	45.83	0.85
EUL ($\overline{w'w'w'} = 0$)	0.86	−11.65	40.69	0.87
HEL ($\overline{w'w'w'} = 0$)	0.90	−14.21	45.51	0.89

The regression model is of the form $y = Ax + B$, where y is the modeled and x is the measured heat flux (in W m^{-2}). The root-mean-square error (rmse) and the correlation coefficient R are also shown.

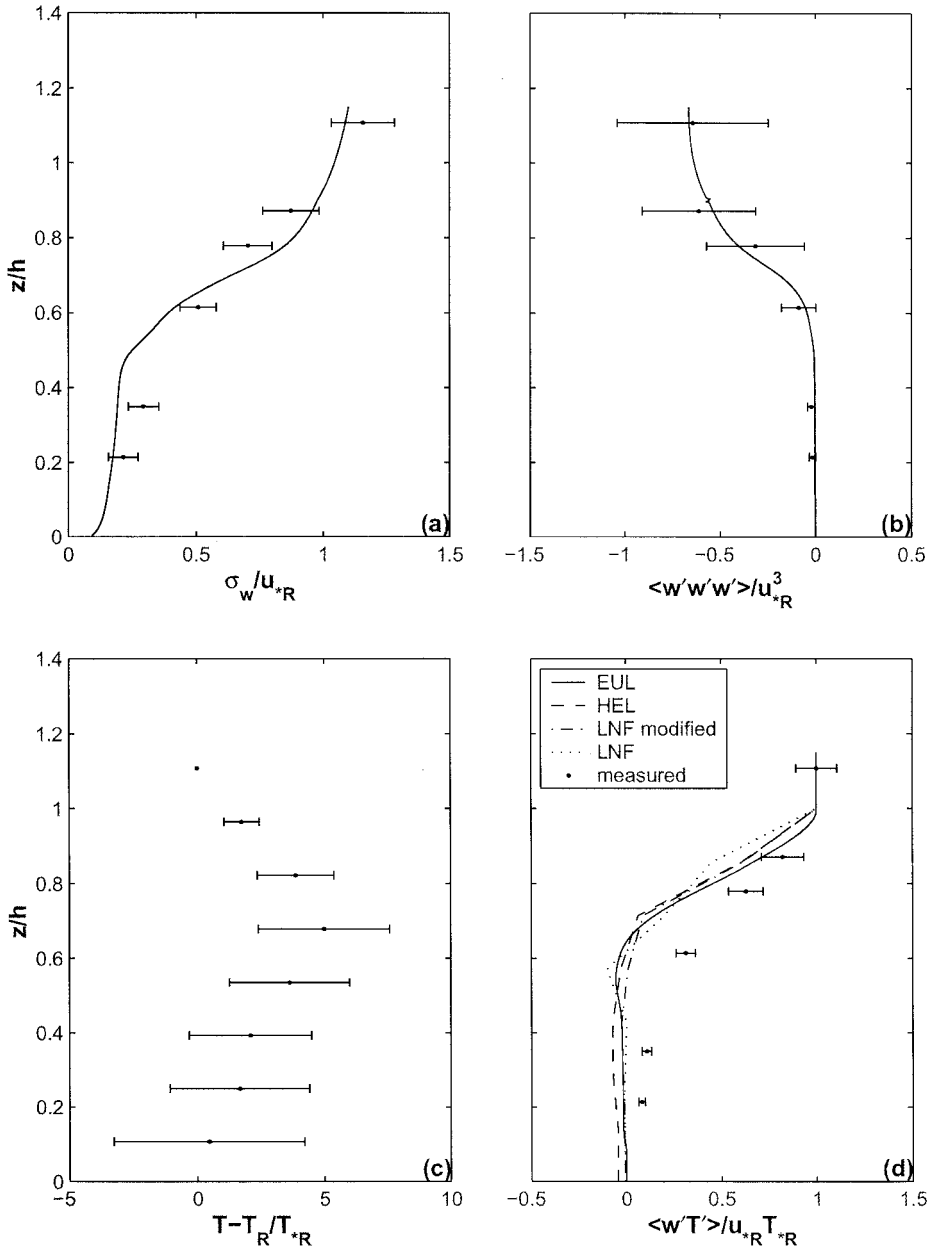

Figure 4. Ensemble vertical distribution for the pine forest heat dispersion experiment. (a) Normalized vertical velocity standard deviation, (b) normalized vertical velocity skewness, (c) normalized temperature difference, and (d) normalized sensible heat flux. The normalizing variables are u_{*R} and h for velocity and length and T_{*R} for temperature, where $T_{*R} = \overline{w'T'_R}/u_{*R}$ and subscript R refers to the variable value at $z/h = 1$.

pared to the measurements in Figure 3. Additionally, the variations of τ and T_L with z/h are displayed for reference. The LNF and HEL sources and fluxes using four and eight layers are computed to assess how sensitive the model results are to the number of layers. In the LNF calculations, the T_L profile, shown in Figure 3, is identical to *Raupach* [1989a] (see Table 1). For the four layer case (Figure 3b), the HEL method better captured the prescribed source profile. However, LNF provided superior agreement between computed and measured sensible flux profiles in comparison to HEL inside the canopy (Figure 3c, Table 2). With eight source layers, LNF resulted in spurious sources in the lower canopy; however, the comparisons between measured and modeled heat flux profiles again suggested superior performance of LNF over HEL (see Table 2, root-mean-square error (rmse)). Among all three methods, the Eulerian approach best reproduced the measured flux profile in terms of regression statistics and minimum rmse (see Table 2). This is not too surprising given that the wind tunnel temperature measurements are collected for "ideal" conditions and do not suffer from uncertainties and errors associated with field measurements.

For the EUL method, the number of grid nodes required to achieve numerical convergence is large (>200 nodes). Hence how the temperature gradients and curvatures are estimated at these nodes from the limited measurements is not unique. Three interpolation schemes that permit numerical and ana-

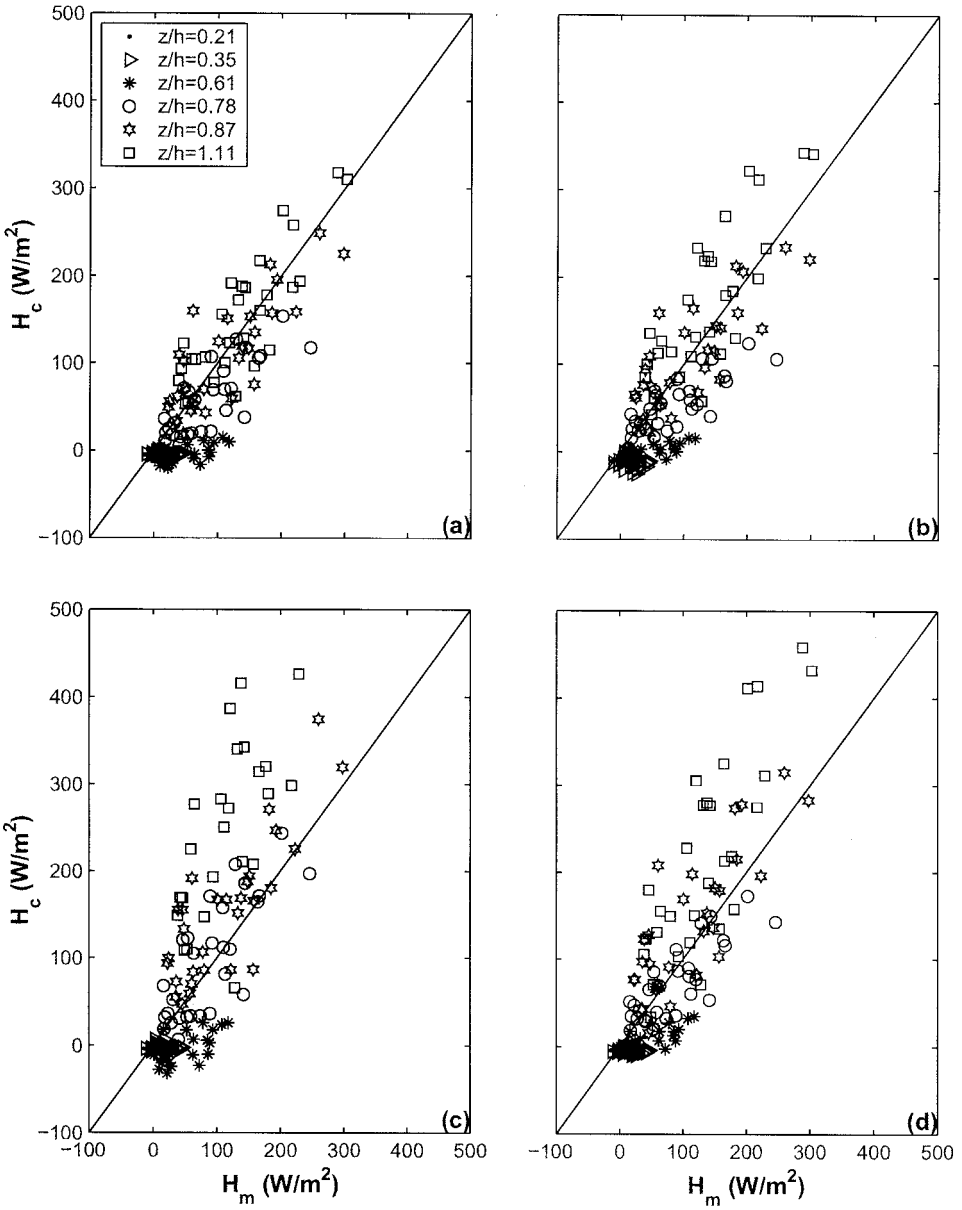

Figure 5. Comparison between measured (H_m) and modeled (H_c) sensible heat fluxes for the pine forest heat dispersion experiment under near-neutral conditions. Different symbols are for different z/h. (a) For EUL, (b) for HEL, (c) for LNF, and (d) for LNF modified with the weighted measures of length procedure presented in Appendix B.

lytical estimation of the temperature gradient from discrete temperature measurements at all grid nodes were experimented. These schemes include (1) fitting the temperature profile to height via an analytical function whose parameters are determined from nonlinear regression analysis, (2) interpolating via cubic spline, and (3) performing local linear regression on consecutive measurement levels to estimate a local temperature gradient (using only three points) and curvature (using only five points). Method 3, the local regression method, was found to be more suitable for such inverse calculations because it best reproduces the measured sources and fluxes and avoids spurious sources near the canopy atmosphere interface [*Katul and Albertson*, 1999]. Additionally, the local regression method is more "portable" since it does not a priori prescribe an analytical form for the temperature distribution. This method was used in the EUL calculations presented in Figure 3 and is adopted throughout this study.

The good agreement noted in Figure 3 and Table 2 for EUL was achieved after the closure constant C_4 was altered from 9.9, used for some canopy flows [*Meyers and Paw U*, 1986, 1987], to 2.0. An uncertainty that impacts the choice of the closure constant C_4 is the estimate of τ from the modeled dissipation rate by *Wilson and Shaw*'s [1977] approach. The dissipation rate was not measured in the *Coppin et al*. [1986] experiment, and hence no direct validation of τ (shown in Figure 3d) is possible. In addition, the estimation of $C_4 = 9.9$ is based on zero scalar flux transport in the surface layer. This assumption may not be reasonable [*Hsieh and Katul*, 1997]. Furthermore, *Moeng and Wyngaard* [1986] demonstrated that $C_4 = 9.9$ is about a factor of 2–3 larger than that estimated for

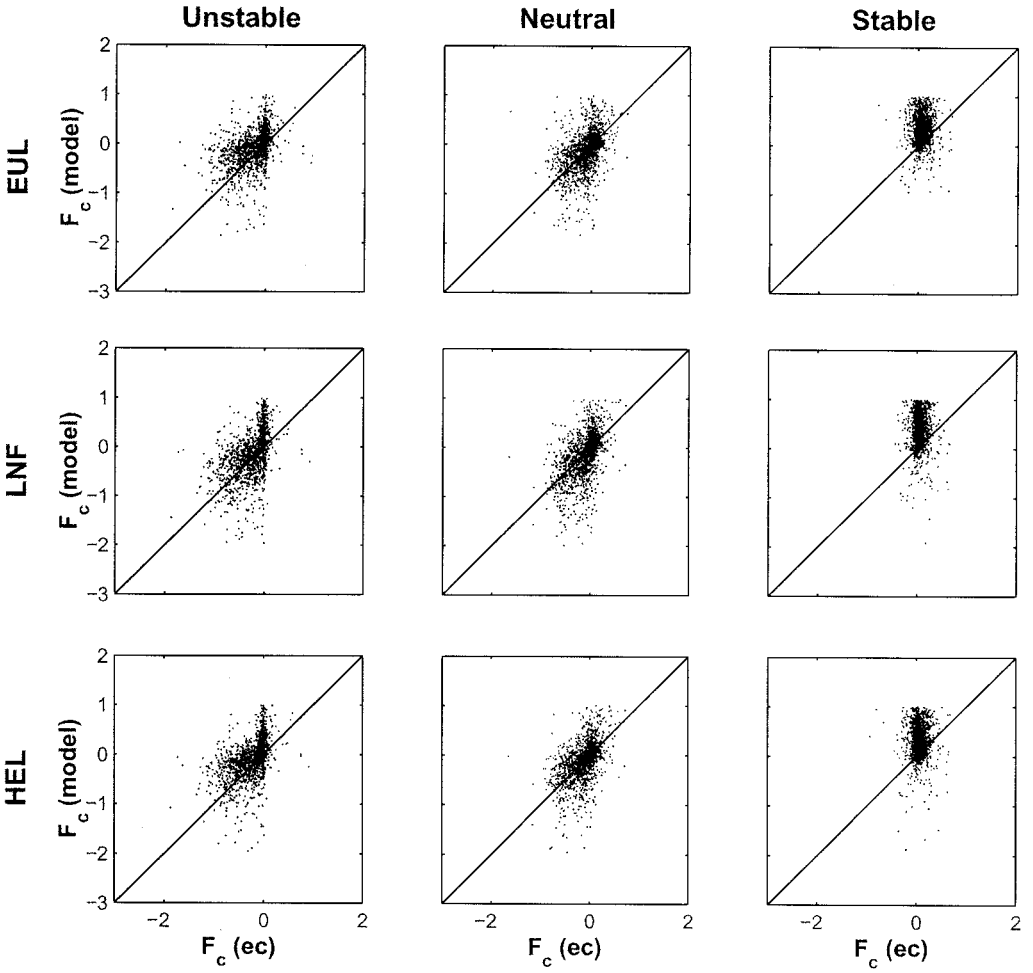

Figure 6. Comparison between eddy-covariance measured ($F_{c(ec)}$) and modeled ($F_{c(\mathrm{model})}$) CO_2 fluxes (F_c in mg m^{-2} s^{-1}) by EUL, LNF, and HEL for unstable, neutral, and stable atmospheric stability conditions. The 1–1 line is also shown.

a convective boundary layer using large eddy simulations. Consequently, the closure constant had to be modified in order to reproduce the sensible heat flux measurements.

Given that *Wilson and Shaw*'s [1977] model failed to reproduce the measured $\langle \overline{w'w'w'} \rangle$, the EUL calculation was repeated assuming $\langle \overline{w'w'w'} \rangle = 0$ for every z. It was found that the EUL model performance did not degrade much with such an approximation (see Table 2).

Having been demonstrated that the performance of the three inverse methods for this ideal wind tunnel study, the performance of these methods in a more complex environment such as forested ecosystems is considered next.

4.2. Duke Forest Heat Dispersion Experiment

An analogous experiment to the wind tunnel was conducted in the field using six sonic anemometers and eight thermocouples. Near-neutral runs were used to assess the attenuation of the sensible heat fluxes within the canopy for a complex heat source distribution. Unlike the wind tunnel experiment, the source distribution was not known; however, the flux distribution within the canopy could be measured. Hence these flux comparisons were used to investigate the three models.

The modeled and measured flow statistics relevant to this comparison are shown in Figure 4a and 4b. The measured flow

Table 4. Comparison Between Measured [F_c (ec)] and Modeled [F_c (model)] CO_2 Fluxes [mg m^{-2} s^{-1}] Above the Canopy

		Stability Conditions		
Method	Criteria	Unstable	Neutral	Stable
LNF modified	retention ratio	0.96	0.95	0.74
	R	0.48	0.50	0.01
	slope	0.75	0.90	0.04
	intercept	−0.04	−0.05	0.34
	rmse	0.44	0.41	0.48
EUL	retention ratio	0.99	0.97	0.88
	R	0.44	0.45	0.05
	slope	0.54	0.70	0.11
	intercept	0.04	−0.04	0.29
	rmse	0.40	0.38	0.39
HEL	retention ratio	0.98	0.97	0.84
	R	0.48	0.50	0.05
	slope	0.63	0.76	0.12
	intercept	0.06	−0.01	0.30
	rmse	0.41	0.36	0.43

The regression model is F_c (model) = Slope F_c (ec) + Intercept. The correlation coefficient (R) and the root-mean-square error (rmse) [mg m^{-2} s^{-1}]) are shown. The numbers of profiles for each stability condition were 1338 for unstable, 1392 for near neutral, and 1685 for stable. The retention ratio is the ratio of runs that satisfied $-2 \leq F_c$ (model) ≤ 1 to the total runs collected.

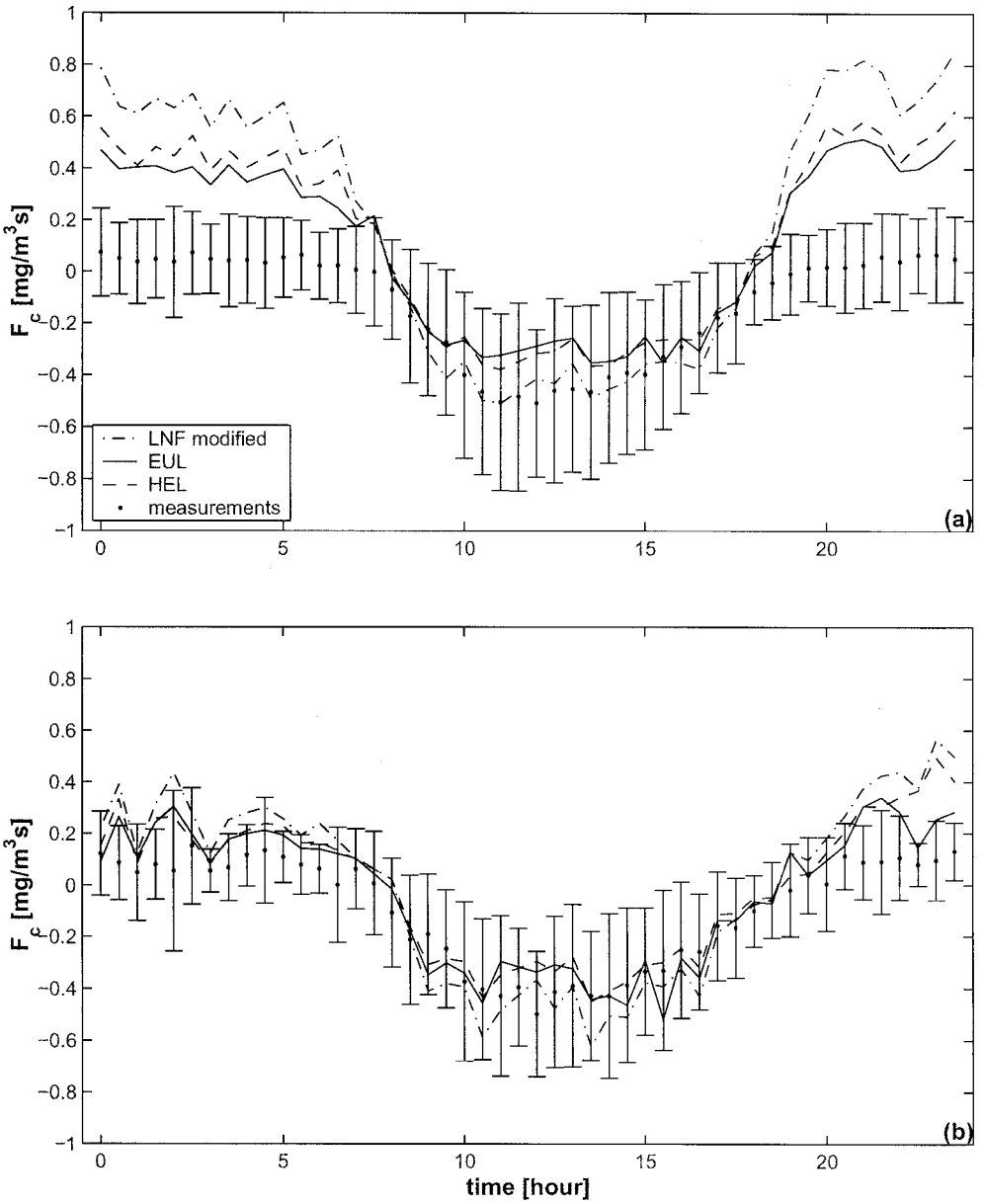

Figure 7. Comparison between measured (dots) and modeled (lines) ensemble-averaged temporal variation of CO_2 fluxes above the canopy. (a) 30 min bins with all stability conditions included in the ensemble average. (b) 30 min bins with only near-neutral condition included in the ensemble average. For reference, one standard deviation of the binned F_c measurements is also shown.

statistics were constructed from the ensemble of 30 neutral runs along with one standard deviation. For each of the 30 runs, the measured temperature profile and the modeled flow statistics were used to compute the flux distribution within the canopy by the three methods. The ensemble-measured and modeled sensible heat fluxes are compared along with one standard deviation of the measured heat flux. For reference, the ensemble temperature profile for all 30 runs is shown along with one standard deviation. As evidenced in Figure 4, all models overattenuated the heat flux inside the canopy. Furthermore, none of the models reproduced well the countergradient heat flux in the lower canopy layers. The measured and modeled sensible heat flux variations at each of the six layers and for all 30 runs are shown in Figure 5. The regression statistics for the three models are also shown in Table 3. The comparison in Table 3 revealed the following:

1. The smoothing constraint introduced in Appendix B significantly improved the original LNF proposed by *Raupach* [1988] (regression slope improved by 20% and rmse reduced by 50%).

2. The hybrid scheme best reproduced a unity regression slope.

3. The Eulerian model, with nonzero skewness, best minimized the rmse.

4. Setting $\langle \overline{w'w'w'} \rangle = 0$ resulted in negligible worsening of the EUL rmse. However, the regression slope was degraded by about 10%.

In short, despite fundamental differences in their deriva-

tions, this analysis suggests that the performance of all three models (LNF modified, HEL, and EUL) is comparable and further supports the findings from the wind tunnel experiments.

4.3. Duke Forest CO_2 Transport Experiments

Using the measured mean CO_2 concentration profiles for each 30 min run and the modeled velocity statistics, the CO_2 sources, sinks, and fluxes within and above the canopy were computed. For LNF and HEL the canopy is divided into seven layers, with the lower layer used to estimate the CO_2 ground flux.

In Figure 6 the computed CO_2 fluxes by these three methods are compared with the eddy covariance fluxes measured above the canopy for three stability classes: unstable, near-neutral, and stable atmospheric stability conditions. From Figure 6 and Table 4 it appears that all three methods poorly reproduce the measured CO_2 fluxes, stable atmospheric conditions being the worst. The best performance for all three models was for near-neutral stability conditions, though the regression statistics leave much to be desired for improved performance for all models (at least on a 30 min time step). To assess the long-term temporal patterns in CO_2 fluxes, the measured and modeled fluxes for every 30 min were ensemble averaged. These bin-averaged results along with one standard deviation on the measurements are shown in Figure 7a without discriminating by stability and Figure 7b for near-neutral conditions only within each 30 min bin. For stable conditions all models overestimated the CO_2 flux (see Figure 7b) even in an ensemble sense. All three models well reproduced the measured temporal flux pattern for near-neutral conditions (Figure 7b). Additionally, the ensemble differences among the models were small, further supporting our findings from the laboratory and field heat dispersion experiments.

In short, while the comparisons suggest all three models reproduce the scalar fluxes with similar skills, HEL offers the potential advantage to replace all Lagrangian quantities needed for computing the dispersion matrix by their Eulerian counterparts.

5. Conclusion

This study demonstrated the following:

1. For the wind tunnel experiments, all three inverse methods well reproduced the measured sensible heat flux profiles even though some differences in their computed source profiles were noted.

2. For the Duke Forest heat dispersion experiment, it was demonstrated that our proposed smoothing constraint on LNF greatly enhanced its performance when contrasted to *Raupach*'s [1988] original version. This smoothing constraint is consistent with *Raupach*'s [1988] assumption of a locally homogeneous source in LNF. The agreement between measured and modeled sensible heat flux within and above the canopy was comparable to all models. None of the three models well reproduced the countergradient flow of heat near the forest floor.

3. For the Duke Forest CO_2 experiments, all three methods overestimate the CO_2 flux at the canopy top for stable atmospheric conditions. Better agreement between eddy-covariance measured and modeled flux was noted for unstable atmospheric conditions. Best agreement was achieved for near-neutral conditions, though the comparisons on 30 min time steps leaves much to be desired about improved model performance. In an ensemble sense, atmospheric stability plays a major role in inverse model calculations and is currently neglected in all three methods.

The broader implication of this study is that despite fundamental differences in model approximations, the computed flux profiles derived from the three methods were very similar. Hence rather than using one approach over the other, it is recommended that all three methods be applied to a particular inverse problem. Agreement among models provides the necessary synergies and confidence that the computed flux is robust to particular model assumptions. However, the close agreement among these models implies that future improvements in inverse methods will not be further enhanced by a one-dimensional steady state, planar homogeneous model of neutral flows.

Appendix A: *Wilson and Shaw*'s [1977] Model

Upon time and horizontally averaging the mean momentum and Reynolds stress equations for neutral conditions, the second-order closure model of *Wilson and Shaw* [1977] reduces to

$$
\begin{aligned}
0 &= -\frac{d\langle\overline{u'w'}\rangle}{dz} - C_d a(z)\langle\bar{u}\rangle^2 \\
0 &= -\langle\overline{w'^2}\rangle\frac{d\langle\bar{u}\rangle}{dz} + 2\frac{d}{dz}\left(q\lambda_1\frac{d\langle\overline{u'w'}\rangle}{dz}\right) - \frac{q\langle\overline{u'w'}\rangle}{3\lambda_2} \\
&\quad + C_w q^2\frac{d\langle\bar{u}\rangle}{dz} \\
0 &= -2\langle\overline{u'w'}\rangle\frac{d\langle\bar{u}\rangle}{dz} + \frac{d}{dz}\left(q\lambda_1\frac{d\langle\overline{u'^2}\rangle}{dz}\right) + 2C_d a(z)\langle\bar{u}\rangle^3 \\
&\quad - \frac{q}{3\lambda_2}\left(\langle\overline{u'^2}\rangle - \frac{q^2}{3}\right) - \frac{2}{3}\frac{q^3}{\lambda_3} \qquad \text{(A1)} \\
0 &= \frac{d}{dz}\left(q\lambda_1\frac{d\langle\overline{v'^2}\rangle}{dz}\right) - \frac{q}{3\lambda_2}\left(\langle\overline{v'^2}\rangle - \frac{q^2}{3}\right) - \frac{2}{3}\frac{q^3}{\lambda_3} \\
0 &= \frac{d}{dz}\left(3q\lambda_1\frac{d\langle\overline{w'^2}\rangle}{dz}\right) - \frac{q}{3\lambda_2}\left(\langle\overline{w'^2}\rangle - \frac{q^2}{3}\right) - \frac{2}{3}\frac{q^3}{\lambda_3}.
\end{aligned}
$$

In (A1), u_i ($u_1 = u$, $u_2 = v$, $u_3 = w$) are the instantaneous velocity components along x_i, x_i ($x_1 = x$, $x_2 = y$, $x_3 = z$) are the longitudinal, lateral, and vertical directions, respectively, λ_1, λ_2, and λ_3 are characteristic length scales for the triple-velocity correlation, the pressure-velocity gradient correlation, and viscous dissipation, respectively, C_w is a constant, k ($= 0.4$) is Von Karman's constant, C_d is the foliage drag coefficient, $a(z)$ is the leaf area density, and a_1, a_2, a_3, and C_w are closure constants that can be determined such that the flow conditions well above the canopy reproduce established surface layer similarity relations. The numerical values of these constants are presented in Table 1 for the wind tunnel and the Duke Forest experiment. The characteristic length scales are defined by

$$
\begin{aligned}
\lambda_j &= a_j L(z); \qquad j = 1, 2, 3, \\
L(z_i) &= \min\begin{cases} L(z_{i-1}) + k\Delta z, \\ \dfrac{\alpha}{C_d a(z_i)}, \end{cases} \\
L(0) &= 0,
\end{aligned}
$$

where α is an empirical constant and $\Delta z = z_i - z_{i-1}$. With estimates of these five constants (a_1, a_2, a_3, C_w, and α), the five ordinary differential equations in (A1) can be solved for the five flow variables $\langle \bar{u} \rangle$, $\langle \overline{u'w'} \rangle$, $\langle \overline{u'^2} \rangle$, $\langle \overline{v'^2}, \rangle$ and $\langle \overline{w'^2} \rangle$ if appropriate boundary conditions are specified. We used the same boundary conditions as those discussed by *Katul and Albertson* [1999] and *Lai et al*. [2000]. While more complex second-order closure schemes [e.g., *Wilson*, 1988] as well as third-order closure schemes have been developed for vegetation flow, recent studies by *Katul and Albertson* [1998] and *Katul and Chang* [1999] suggest that the *Wilson and Shaw* [1977] model performs no worse than *Wilson*'s [1988] and another third-order closure models for this pine forest. We note that the closure constants a_1, a_2, a_3, C_w are dependent on the assumed values of the normalized $\langle \overline{u'^2} \rangle$, $\langle \overline{v'^2} \rangle$, and $\langle \overline{w'^2} \rangle$ in the atmospheric surface layer and are independent on the canopy morphology. The constants α and C_d are dependent on the canopy morphology and can vary for different canopies. For vegetation, C_d varies from 0.15 to 0.3 and α varies from 0.02 to 0.07.

Appendix B: Weighted Measure of Length Procedure

The details of this algorithm are described by *Menke* [1989]. However, for completeness, the key steps are reviewed. An inverse problem can be stated in an explicit linear matrix form as: $\mathbf{Gm} = \mathbf{d}$, where $\mathbf{G}$ is the sensitivity matrix, $\mathbf{m}$ is the model parameter vector, and $\mathbf{d}$ is the data vector.

A standard technique to avoid discontinuities in the source profile is to use difference between physically adjacent model parameters as approximations of first derivative. The implementation of this procedure in a least squares sense is to include a measure of the flatness of the parameter vector in the minimization calculation. The flatness $\mathbf{l}$ is defined as

$$\mathbf{l} = \begin{bmatrix} -1 & 1 & 0 & \cdots & \cdots & 0 \\ 0 & -1 & 1 & 0 & \cdots & 0 \\ \vdots & & \ddots & \ddots & & \vdots \\ 0 & \cdots & 0 & -1 & 1 & 0 \\ 0 & \cdots & \cdots & 0 & -1 & 1 \end{bmatrix} \begin{bmatrix} m_1 \\ m_2 \\ \vdots \\ m_{M-1} \\ m_M \end{bmatrix} = \mathbf{Fm}. \quad \text{(B1)}$$

The overall flatness of the solution is the length

$$L = \mathbf{l}^T\mathbf{l} = [\mathbf{Fm}]^T[\mathbf{Fm}] = \mathbf{m}^T\mathbf{F}^T\mathbf{Fm} = \mathbf{m}^T\mathbf{W}_m\mathbf{m}. \quad \text{(B2)}$$

The matrix $\mathbf{W}_m$ in (B2) can be interpreted as a weighting factor. The quantity to be minimized should now be a combination of the prediction error and length L and can be defined as

$$\Phi(\mathbf{m}) = E + \varepsilon^2 L = \mathbf{e}^T\mathbf{e} + \varepsilon^2\mathbf{m}^T\mathbf{W}_m\mathbf{m}. \quad \text{(B3)}$$

In the minimization of Φ with respect to model parameters, the following matrix equation is obtained:

$$\mathbf{m}^{\text{est}} = [\mathbf{G}^T\mathbf{G} + \varepsilon^2\mathbf{W}_m]^{-1}\mathbf{G}^T\mathbf{d}, \quad \text{(B4)}$$

where $\mathbf{m}^{\text{est}}$ is the desired estimated model parameter vector (in this case, the source S_j), $\mathbf{G}$ is the matrix defined by $D_{ij}\Delta z_j$, where D_{ij} is, as before, the dispersion matrix, and $\mathbf{d}$ is the concentration difference ($= \langle \bar{c} \rangle_i - \langle \bar{c} \rangle_R$) vector.

Acknowledgments. The authors would like to thank Karen Wesson and Cheng-I Hsieh for their helpful comments on the manuscript. The first author is supported by the Conselho Nacional de Desenvolvimento Científico e Tecnólogico (CNPq) of Brazil. Additional support was provided by the National Science Foundation (NSF-BIR 95-12333 and NSF-EAR 99-03471), the Department of Energy (DOE) through the FACE-FACTS project, and through the National Institute of Global Environmental Change (NIGEC) through the Southeast Regional Center at the University of Alabama, Tuscaloosa (DOE cooperative agreement DE-FC030-90ER61010).

References

Anthoni, P. M., B. E. Law, and M. H. Unsworth, Carbon and water vapor exchange of an open-canopied ponderosa pine ecosystem, *Agric. For. Meteorol*., *95*, 151–168, 1999.

Baldocchi, D., and P. C. Harley, Scaling carbon dioxide and water vapor exchange from leaf to canopy in a deciduous forest, II, Model testing and application, *Plant Cell Environ*., *18*, 1157–1173, 1995.

Baldocchi, D., and T. Meyers, On the eco-physiological and biogeochemical theory to evaluate carbon dioxide, water vapor and trace gas fluxes over vegetation: A perspective, *Agric. For. Meteorol*., *90*, 1–25, 1998.

Blanken, P. D., T. A. Black, H. H. Neumann, G. Den Hartog, P. C. Yang, Z. Neisc, R. Staebler, and W. Chen, Turbulent flux measurements above and below the overstory of a boreal aspen forest, *Boundary Layer Meteorol*., *89*, 109–140, 1998.

Coppin, P. A., M. R. Raupach, and B. J. Legg, Experiments on scalar dispersion within a model canopy, part II, An elevated plane source, *Boundary Layer Meteorol*., *35*, 167–191, 1986.

Culf, A. D., G. Fisch, Y. Malhi, and C. A. Nobre, The influence of the atmospheric boundary layer on carbon dioxide concentrations over a tropical forest, *Agric. For. Meteorol*., *85*, 149–158, 1997.

Denmead, O. T., Novel meteorological methods for measuring trace gas fluxes, *Philos. Trans. R. Soc. London*, *Ser. A*, *351*, 383–396, 1995.

Denmead, O. T., and E. F. Bradley, Flux-gradient relationships in a forest canopy, in *The Forest-Atmosphere Interaction*, edited by B. A. Hutchinson and B. B. Hicks, pp. 421–442, D. Reidel, Norwell, Mass., 1985.

Finnigan, J. J., Turbulent transport in plant canopies, in *The Forest-Atmosphere Interaction*, edited by B. A. Hutchinson and B. B. Hicks, pp. 443–480, D. Reidel, Norwell, Mass., 1985.

Gao, W., M. L. Wesely, and P. V. Doskey, Numerical modeling of the turbulent diffusion and chemistry of NO_x, O_3, isoprene, and other reactive trace gases in and above a forest canopy, *J. Geophys. Res*., *98*, 18,339–18,353, 1993.

Gu, L. H., Comments on "A practical method for relating scalar concentrations to source distributions in vegetation canopies" by M. R. Raupach, *Boundary Layer Meteorol*., *87*, 515–524, 1998.

Gu, L. H., H. H. Shugart, J. D. Fuentes, T. A. Black, and S. R. Shewchuk, Micrometeorology, biophysical exchange and NEE decomposition in a two-story boreal forest—Development and test of an integrated model, *Agric. For. Meteorol*., *94*, 123–148, 1999.

Hsieh, C. I., and G. G. Katul, Dissipation methods, Taylor's hypothesis, and stability correction functions in the atmospheric surface layer, *J. Geophys. Res*., *102*, 16,391–16,405, 1997.

Kaimal, J. C., and J. J. Finnigan, *Atmospheric Boundary Layer Flows: Their Structure and Measurement*, 289 pp., Oxford Univ. Press, New York, 1994.

Katul, G. G., and J. D. Albertson, An investigation of higher order closure models for a forested canopy, *Boundary Layer Meteorol*., *89*, 47–74, 1998.

Katul, G. G., and J. D. Albertson, Modeling CO_2 sources, sinks, and fluxes within a forest canopy, *J. Geophys. Res*., *104*, 6081–6091, 1999.

Katul, G. G., and W.-H. Chang, Principal length scales in second-order closure models for canopy turbulence, *J. Appl. Meteorol*., *38*, 1631–1643, 1999.

Katul, G. G., R. Oren, D. Ellsworth, C. I. Hsieh, N. Phillips, and K. Lewin, A Lagrangian dispersion model for predicting CO_2 sources, sinks, and fluxes in a uniform loblolly pine (*Pinus taeda L*.) stand, *J. Geophys. Res*., *102*, 9309–9321, 1997a.

Katul, G. G., C. I. Hsieh, G. Kuhn, D. Ellsworth, and D. Nie, Turbulent eddy motion at the forest-atmosphere interface, *J. Geophys. Res*., *102*, 13,409–13,421, 1997b.

Katul, G. G., et al., Spatial variability of turbulent fluxes in the roughness sublayer of an even-aged pine forest, *Boundary Layer Meteorol*., *93*, 1–28, 1999.

Katul, G. G., R. Leuning, J. Kim, O. T. Denmead, A. Miyata, and Y.

Harazono, Estimating CO_2 source/sink distributions within a rice canopy using higher-order closure models, *Boundary Layer Meteorol*., in press, 2000.

Lai, C. T., G. G. Katul, D. Ellsworth, and R. Oren, Modelling vegetation-atmosphere CO_2 exchange by a coupled Eulerian-Lagrangian approach, *Boundary Layer Meteorol*., *95*, 91–122, 2000.

Law, B. E., D. D. Baldocchi, and P. M. Anthoni, Below-canopy and soil CO_2 fluxes in a ponderosa pine forest, *Agric. For. Meteorol*., *94*, 171–188, 1999.

Lee, X. H., On micrometeorological observations of the surface-air exchange over tall vegetation, *Agric. For. Meteorol*., *91*, 39–49, 1998.

Malhi, Y., A. D. Nobre, J. G. Grace, B. Kruijt, M. G. P. Pereira, A. Culf, and S. Scott, Carbon dioxide transfer over a central Amazonian rain forest, *J. Geophys. Res*., *103*, 31,593–31,612, 1998.

Massman, W. J., and J. C. Weil, An analytical one-dimensional second-order closure model of turbulence statistics and the Lagrangian timescale within and above plant canopies of arbitrary structure, *Boundary Layer Meteorol*., *91*, 81–107, 1999.

Menke, W., Geophysical data analysis: Discrete inverse theory, in *International Geophysical Series*, vol. 45, rev. ed., pp. 52–53, Academic, San Diego, Calif., 1989.

Meyers, T., and K. T. Paw U, Testing of a higher-order closure model for modeling airflow within and above plant canopies, *Boundary Layer Meteorol*., *37*, 297–311, 1986.

Meyers, T., and K. T. Paw U, Modeling the plant canopy micrometeorology with higher-order closure principles, *Agric. For. Meteorol*., *41*, 143–163, 1987.

Moeng, C. H., and J. C. Wyngaard, An analysis of the pressure-scalar covariances in the convective boundary layer, *J. Atmos. Sci*., *43*, 2499–2513, 1986.

Potosnak, M., S. C. Wofsy, A. S. Denning, T. J. Conway, J. W. Munger, and D. H. Barnes, Influence of biotic exchange and combustion sources on atmospheric CO_2 concentrations in New England from observations at a forest flux tower, *J. Geophys. Res*., *104*, 9561–9569, 1999.

Rannik, U., On the surface similarity at a complex forest site, *J. Geophys. Res*., *103*, 8685–8697, 1998.

Raupach, M. R., Canopy transport processes, in *Flow and Transport in the Natural Environment*, edited by W. L. Steffen, and O. T. Denmead, pp. 95–127, Springer-Verlag, New York, 1988.

Raupach, M. R., Applying Lagrangian fluid mechanics to infer scalar source distributions from concentration profiles in plant canopies, *Agric. For. Meteorol*., *47*, 85–108, 1989a.

Raupach, M. R., A practical Lagrangian method for relating scalar concentrations to source distributions in vegetation canopies, *Q. J. R. Meteorol. Soc*., *115*, 609–632, 1989b.

Raupach, M. R., Response to Gu (1998), "Comments to 'A practical Lagrangian method for relating scalar concentrations and source distributions in plant canopies' by M. R. Raupach (1989)", *Boundary Layer Meteorol*., *87*, 525–528, 1998.

Raupach, M. R., and R. H. Shaw, Averaging procedures for flow within vegetation canopies, *Boundary Layer Meteorol*., *22*, 79–90, 1982.

Raupach, M. R., O. T. Denmead, and F. X. Dunin, Challenges in linking atmospheric CO_2 concentrations to fluxes at local and regional scales, *Aust. J. Bot*., *40*, 697–716, 1992.

Raupach, M. R., J. J. Finnigan, and Y. Brunet, Coherent eddies and turbulence in vegetation canopies: The mixing-layer analogy, *Boundary Layer Meteorol*., *78*, 351–382, 1996.

Simpson, I. J., G. W. Thurtell, H. H. Neumann, G. Den Hartog, and G. C. Edwards, The validity of similarity theory in the roughness sublayer above forest, *Boundary Layer Meteorol*., *87*, 69–99, 1998.

Thomson, D. J., Criteria for the selection of stochastic models of particle trajectories in turbulent flows, *J. Fluid Mech*., *180*, 529–556, 1987.

Vermetten, A. W. M., L. Ganzeveld, A. Jeuken, P. Hofschreuder, and G. M. J. Mohren, CO_2 uptake by a stand of Douglas-fir—Flux measurements compared with model-calculations, *Agric. For. Meteorol*., *72*, 57–80, 1994.

Wilson, J. D., A second order closure model for flow through vegetation, *Boundary Layer Meteorol*., *42*, 371–392, 1988.

Wilson, J. D., Turbulent transport within the plant canopy, in *Estimation of Areal Evapotranspiration*, *IAHS Publ*., *177*, 43–80, 1989.

Wilson, N. R., and R. H. Shaw, A higher order closure model for canopy flow, *J. Appl. Meteorol*., *16*, 1198–1205, 1977.

Wofsy, S. C., M. L. Goulden, J. W. Munger, S. M. Fan, P. S. Bakwin, B. C. Daube, S. L. Bassow, and F. A. Bazzaz, Net exchange of CO_2 in a mid-latitude forest, *Science*, *260*, 1314–1317, 1993.

G. Katul, C.-T. Lai, and M. Siqueira, School of the Environment, Box 90328, Duke University, Durham, NC 27708-0328. (mbs@duke.edu)

(Received September 3, 1999; revised August 16, 2000;
accepted August 19, 2000.)